

Model predictive control-based DC overcurrent protection method for 400 Hz ground power unit

Son Tran Que^{1,2}, Vuong Nguyen Anh³, Diep Huynh Van³, Dich Nguyen Quang¹, Trung Nguyen Kien³

¹Institute for Control Engineering and Automation, Hanoi University of Science and Technology, Hanoi, Vietnam

²Faculty of International Training, Thai Nguyen University of Technology, Thai Nguyen, Vietnam

³School of Electrical and Electronic Engineering, Hanoi University of Science and Technology, Hanoi, Vietnam

Article Info

Article history:

Received Jul 5, 2024

Revised Dec 2, 2024

Accepted Dec 9, 2024

Keywords:

DC overcurrent protection

Ground power unit

Lithium battery model

Model predictive control

Proportional resonant control

ABSTRACT

This paper presents a new configuration of 400 Hz inverters designed for ground power units (GPU) in the aerospace field. In this model, instead of using rectifiers fed by the AC electric grid, a lithium battery system is employed due to its advantages, especially in improving the flexibility and reliability of the power supply. A model predictive control (MPC) strategy with the extended cost function is proposed for the current loop, which is expected to restrict the DC current avoiding the battery overcurrent that causes the system interrupted by the battery management system (BMS), improving the overall system dynamic. The mathematical relationship between battery current and inductor current has also been derived to support the design of the MPC controller. A proportional resonant (PR) controller is performed for the outer loop to control fundamental voltages, and compensate for the harmonic distortions. A comprehensive simulation model is initially created in the MATLAB environment and subsequently validated through hardware-in-the-loop (HIL) testing to assess the performance of the proposed control technique. The results obtained demonstrate the effectiveness of the control scheme in terms of DC-link battery current being controlled at an acceptable value, high-quality voltage is provided at the output with harmonic distortions compensated by PR controller.

This is an open access article under the [CC BY-SA](https://creativecommons.org/licenses/by-sa/4.0/) license.



Corresponding Author:

Trung Nguyen Kien

School of Electrical and Electronic Engineering, Hanoi University of Science and Technology

Dai Co Viet, Hai Ba Trung, Hanoi, Vietnam

Email: trung.nguyenkien1@hust.edu.vn

1. INTRODUCTION

The airline industry has seen significant growth in both civil and military areas in recent time. Airport regulations now mandate the use of external power units to energize aircraft while parked, aimed at minimizing noise and reducing air pollution. This has led to a continuous increase in demand for ground power units (GPUs), which provide external power to aircraft when they are stationed at the airport. The typical voltage requirement for GPUs is 115 V RMS at a frequency of 400 Hz. A primary objective in GPU design is to maintain the total harmonic distortion (THD) under 2.5%, even when powering unbalanced and nonlinear loads [1].

Traditionally, GPUs have been constructed with an input AC-DC converter, an inverter, a transformer, and output filters. Even so, this conventional approach results in a bulky, heavy, and difficult-to-install system. Additionally, the rectifier input stage requires complex filtering to mitigate harmonic distortions. To address these drawbacks, the proposed GPU design in this paper replaces the traditional rectifier input with a lithium battery system. This change enhances the system's flexibility and reliability. Furthermore, the output filter

inductor is integrated into the isolated transformer's leakage, which helps reduce the overall weight and volume of the GPU system [2].

One significant limitation of a lithium battery-powered inverter is that the DC overcurrent is controlled by the BMS. If the DC current exceeds a certain threshold, the BMS will automatically shut down the DC power supply to protect the battery cells [3]-[8]. The reason for this is that lithium-ion batteries are sensitive to overcurrent, which can lead to overheating, thermal runaway, and potentially even fire or explosion [9]-[12]. This means that the inverter will lose its power source and will no longer be able to function, potentially leading to a disruption in the power supply. By addressing this critical limitation, a control system design is required that can maintain reliable and uninterrupted power supply, even in the face of temporary overcurrent conditions. This is a significant focus area in the ongoing efforts in this research to improve the proposed lithium battery-powered GPU's performance and safety. Controlling the DC current directly is complicated, an effective approach is to manage the load current indirectly by maintaining the inductor current. To successfully apply this control strategy, it is essential to define the relationship between the lithium battery current and the inductor current. The primary contribution of this study is the formulation of a mathematical equation that illustrates the connection between the lithium battery current and the inductor current, along with the inverter switching state, which serves for the current control loop design in this paper, and for other research directions on controlling the DC overcurrent for battery-powered inverter.

Currently, several control methods have been developed for inverters. Among the most common are single-loop control and cascade-loop control. The single loop control method [13]-[18] is characterized by its straightforward design of control parameters, and its implementation is relatively low-cost as it requires only a single voltage sensor. But, the primary disadvantage of single-loop control is its susceptibility to instability and its inability to regulate current. As a result, output voltage is vulnerable to shut off state, due to the DC battery overcurrent, when considered to the proposed GPU in this paper. To address these issues and enhance robustness while providing immunity to disturbances and current protection, cascade loop control is more advantageous. In contrast to single loop control, cascade loop control incorporates an additional inner loop, typically the inductor current loop. The inductor current is monitored and utilized to regulate the duty cycle [19]-[21].

The model predictive control (MPC) technique is a straightforward and effective approach that relies on the model of the controlled system to forecast its future behavior and determine the optimal control action based on a defined optimality criterion. This strategy leverages the inherent discrete nature of power converters and the limited switching states to address optimization problems by predicting system behavior solely for those feasible switching states [22]-[31]. Each prediction is then used to assess a cost function, allowing for the selection of the state with the lowest cost to be executed [26]-[31]. Additionally, it offers several appealing features, including design simplicity, rapid dynamic response, and the capability to incorporate nonlinearities and constraints into the controller design. Furthermore, the MPC strategy eliminates the need for a pulse width modulation (PWM) modulation stage and facilitates the inclusion of constraints in the MPC cost function to achieve specific control goals.

The secondary contribution of this research is the introduction of a novel current control scheme that maintains the inductor current within the desired operating range, to proactively manage the DC current to stay below the threshold value that would trigger the BMS to shut down the system. In order to implement effective control over the overcurrent condition, there is a trade-off that must be reached between maintaining the output voltage quality and the ability to limit the current. This reflects the challenge in designing the control system, as there is a balance that needs to be struck between these two competing objectives - high-quality output voltage and robust overcurrent limitation. To manage this trade-off, the MPC approach has been chosen as the control method, whose cost function has been expanded to include the DC current constraint. For the voltage loop, a traditional PR controller with a phase delay compensation technique has been applied due to its high performance in achieving zero steady-state tracking error, and compensating for harmonic distortion [32], [33].

2. DC OVERCURRENT PROTECTION TECHNIQUE BASED ON MPC

2.1. Lithium-ion battery equivalent circuit

Lithium-ion battery circuit model depicted in Figure 1 comprises three components: i) the internal ohmic resistor R_s ; ii) a parallel arrangement of a resistor and capacitor, C_p/R_p , where R_p represents the equivalent polarization resistance and C_p denotes the equivalent polarization capacitance, which is utilized to model the battery's transient behavior during charging and discharging events; and iii) the open-circuit voltage $v_{oc}(h(t))$, which is a nonlinear function dependent on the state of charge $h(t)$. The current is treated as the control input, while the terminal voltage is regarded as the output measurement [34]. Based on Kirchhoff's law, the above circuit dynamic equation is derived as (1).

$$\begin{cases} \hat{v}_b(t) = \hat{v}_{oc}(h(t)) - R_s \hat{i}_b(t) - \hat{v}_c(t) \\ \frac{d\hat{v}_c(t)}{dt} = -\frac{1}{C_p R_p} \hat{v}_c(t) + \frac{1}{C_p} \hat{i}_b(t) \end{cases} \quad (1)$$

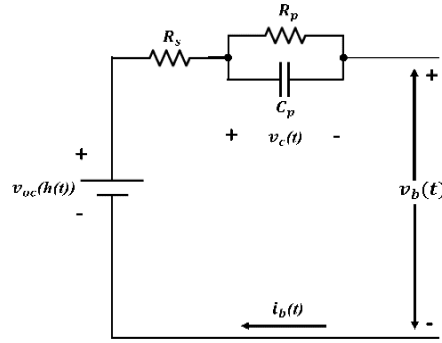


Figure 1. The lithium-ion battery equivalent circuit

2.2. MPC current loop control design

The overall control structure is shown in Figure 2. The inverter dynamic equation is provided as (2).

$$v_{inv}(t) = r_L i_L(t) + L \frac{di_L(t)}{dt} + v_o(t) \quad (2)$$

In which, $v_{inv}(t)$ is H-bridge output voltage, r_L is inductor resistance. With $S_1(t)$, $S_2(t)$, $S_3(t)$, $S_4(t)$ are state of valves, the switching state function can be expressed as (3).

$$\phi(t) = S_1(t)S_4(t) - S_2(t)S_3(t) \quad (3)$$

The inverter output voltage can also be expressed as (4).

$$v_{inv}(t) = \phi(t)\hat{v}_b(t) \quad (4)$$

Apply the Euler approximation, as in (5).

$$\frac{di_L(t)}{dt} \approx \frac{i_L(k+1) - i_L(k)}{T_s} \quad (5)$$

Substitute (5) to (2), leading to (6).

$$i_L(k+1) = \left(1 - \frac{r_L T_s}{L}\right) i_L(k) + \frac{T_s}{L} [v_{inv}(k) - v_o(k)] \quad (6)$$

Or, as in (7).

$$\frac{T_s}{L} v_{inv}(k) = i_L(k+1) - \left(1 - \frac{r_L T_s}{L}\right) i_L(k) + \frac{T_s}{L} v_o(k) \quad (7)$$

Which can be rewritten as (8).

$$v_{inv}(k) = \left[i_L(k+1) - \left(1 - \frac{r_L T_s}{L}\right) i_L(k) + \frac{T_s}{L} v_o(k) \right] \frac{L}{T_s} \quad (8)$$

From (1), it can be derived as (9).

$$\hat{i}_b(k) = \frac{\hat{v}_{oc}(h(k)) - \hat{v}_c(k) - \hat{v}_b(k)}{R_s} \quad (9)$$

From (8) and (9), the input DC battery current can be estimated as (10).

$$\hat{i}_b(k) = \frac{\hat{v}_{oc}(h(k)) - \hat{v}_c(k) - \left[i_L(k+1) - \left(1 - \frac{r_L T_s}{L}\right) i_L(k) + \frac{T_s}{L} v_o(k) \right] \frac{L}{T_s} V_i(k)}{R_s} \quad (10)$$

In which, $V_i(k)$ is a state function, which can be -1, 0, or 1. All possible switching states and corresponding voltages are provided in Table 1.

Finally, the cost function g can be formulated as (11).

$$g = [i_L^*(k) - i_L(k+1)]^2 + \lambda \quad (11)$$

In which, λ is the weighting factor, which is defined as (12).

$$\begin{cases} \lambda = 0 & \text{for } \hat{i}_b(k) < I_b^* \\ \lambda = \infty & \text{else} \end{cases} \quad (12)$$

In this context, $i_L^*(k)$ represents the reference current, while I_b^* denotes the maximum discharge current of the lithium battery, which is specified as 130 A for the proposed battery system.

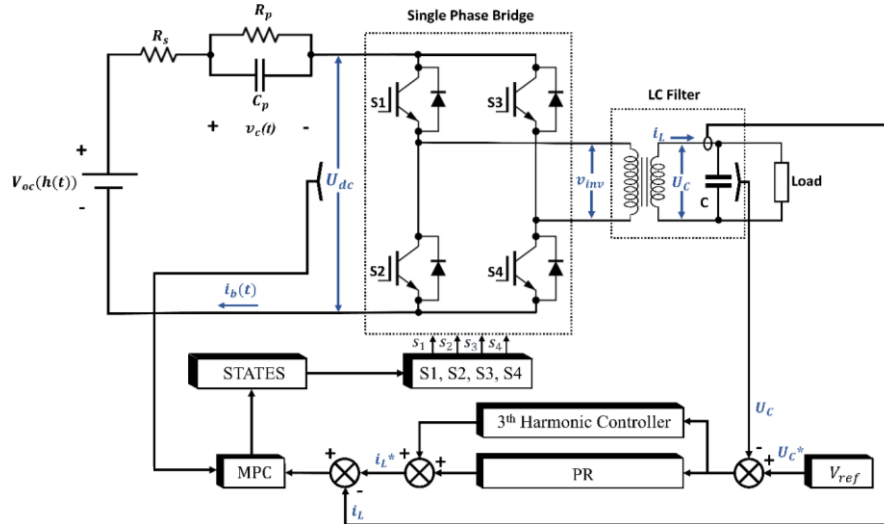


Figure 2. The power system with lithium battery is expressed by its equivalent circuit

Table 1. The possible switching states

Gate states	S ₁	S ₂	S ₃	S ₄	$\phi(t)$	v_o
State 1	1	0	1	0	0	0
State 2	0	1	0	1	0	0
State 3	1	0	0	1	1	Vdc
State 4	0	1	1	0	-1	-Vdc

Figure 3 indicates the distribution of the DC current in H-bridge circuit, with the red line representing the DC current drawn from the battery to the load, and the blue line representing the DC current returning from the load to the input DC capacitor, during the two halves of the output voltage cycle across the load. The diagram in Figure 4 depicts the process of the proposed MPC current loop. By utilizing the measured values of the filter current $i_L(k)$, inverter output voltage $v_{inv}(k)$, and output voltage $v_o(k)$, MPC algorithm calculates the predicted value of the inductor current $i_L(k+1)$ for all possible switching state scenarios. Additionally, the DC battery current $\hat{i}_b(k)$ is estimated for each switching state, as shown in Table 1. Subsequently, an extended cost function is evaluated to determine the optimal switching state. The optimal switching state is then implemented in the subsequent sampling period, with the switching pulses generated by the MPC according to the chosen switching state.

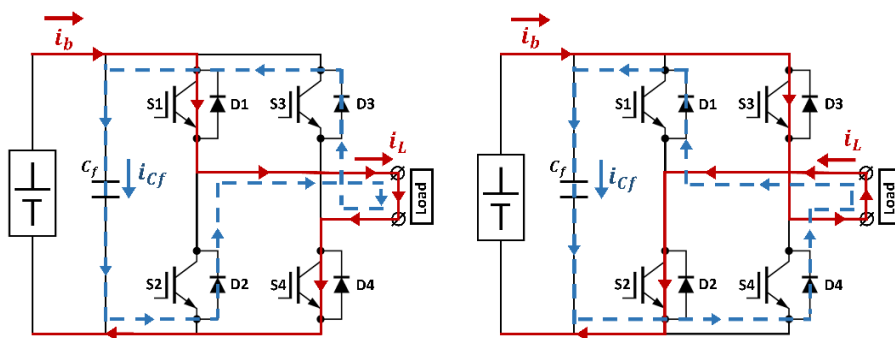


Figure 3. The DC current drawn from battery system

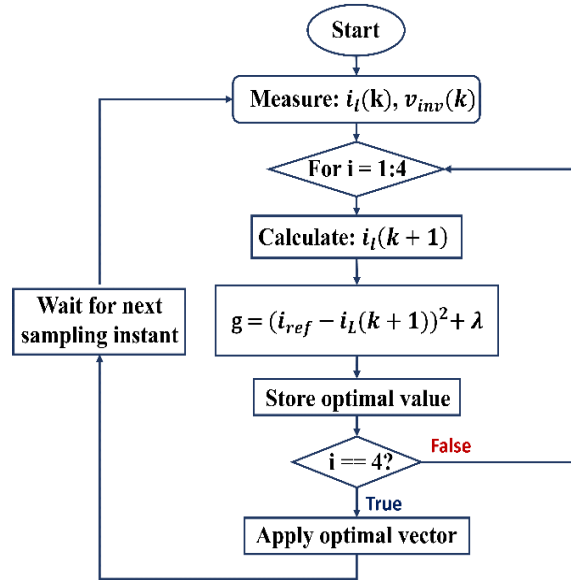


Figure 4. Flowchart of MPC control

3. OUTER LOOP VOLTAGE CONTROL DESIGN

3.1. Discrete resonant controller with phase compensation technique

The continuous time PR controller function is as (13) [32].

$$G_{PR}^c(s) = 2K_p + K_r \frac{\cos(\theta_d)s - h\omega_0 \sin(\theta_d)}{s^2 + (h\omega_0)^2} \quad (13)$$

In which K_r is resonant gain and θ_d refers to the angles used to adjust the phase delay. Each phase of the compensator can be modified by varying θ_d in (13). In this research, θ_d is determined based on the phase angle of the system's open-loop frequency response. Finally, by applying zero order hold (ZOH) transform, a discrete model of the PR controller can be obtained as (14).

$$G_{PR}^d(z) = 2K_p + K_r T_s \frac{[\cos(\theta_d) - h\omega_0 T_s \sin(\theta_d)]z - \cos(\theta_d)}{z^2 + (h^2 \omega_0^2 T_s^2 - 2)z + 1} \quad (14)$$

With the sampling frequency is 18 kHz, the discrete fundamental PR controller function is as (15).

$$G_{PR}^d(1) = \frac{0.7854z^2 - 1.518z + 0.7468}{z^2 - 1.981z + 1} \quad (15)$$

To assess the relative system stability, the Bode diagram of the closed-loop transfer function is obtained under no-load conditions. It is important to note that the no-load condition typically represents the worst-case scenario, as the system exhibits its lowest damping value. Figure 5(a) depicts the system response when the fundamental PR controller is applied. It can be observed that the system achieves satisfactory gain and phase margins, and the resonance is located at approximately 400 Hz, which is the desired frequency.

The system frequency response is continued to investigated in the case of third order harmonic compensator is implemented to the PR controller. Firstly, the third-order PR controller function can be easily obtained by substituting $h = 3$ to the (14), which can be expressed in (16).

$$G_{PR}^d(3) = \frac{0.08365z - 0.1564}{z^2 - 1.825z + 1} \quad (16)$$

It is shown by Figure 5(b) that when the 3rd harmonic compensator is added, the system stability remains, with the gain and phase margin still good, and the resonance peak is close to 400 Hz and 1200 Hz as expected.

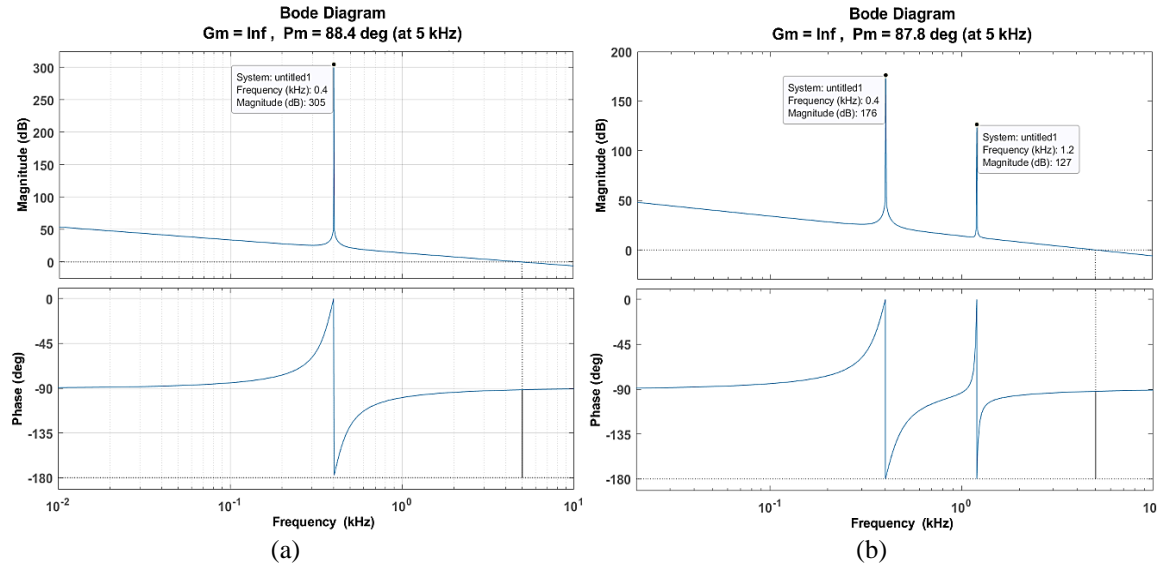


Figure 5. System frequency response: (a) fundamental controller and (b) with 3rd harmonic compensator added

4. A CASE STUDY

4.1. The GPU parameters

To assess the feasibility of the proposed approach, simulations are conducted using MATLAB/Simulink and HIL techniques. System parameters provided in Table 2 are utilized for the subsequent analyses. The results of the simulations will be discussed in the following section.

4.2. Simulation results

MATLAB simulations the initial simulation scenario features a linear load, utilizing only the fundamental PR controller for the voltage loop. As depicted in Figure 6, the output voltage is maintained at the desired setpoint value within 0.01 seconds, with excellent synchronization, suggesting that the steady-state error is near zero. The THD content is kept at sufficiently small value, which is just 1.03%.

The next simulation investigates the system response under no-load conditions. The THD of the output voltage is 1.29%, as illustrated in Figure 7, where only the fundamental PR controller is utilized for the outer voltage loop. Additionally, similar to the previous simulation, the impact of harmonics on the output voltage is sufficiently minimal in this case, indicating that harmonic compensation controllers are unnecessary within the PR controller.

Table 2. System parameters

Parameter	Value
DC voltage	400 V
Filter inductance	200 μ H
Filter capacitance	25 μ F
Inductor resistance	0.02 Ω
PWM frequency	18 kHz
Frequency	400 Hz

The proposed control system is further examined for the switching load condition, where the full load is connected at 0.055s. The results shown in Figure 8 demonstrate the fast recovery of the output voltage and inductor current under the load change. Despite the load transition, the output voltage THD remains at 1.62%, and the high-order harmonic components are minimal, even without the use of harmonic compensators. This indicates the effectiveness of the proposed control system in maintaining a stable and high-quality output under dynamic load conditions.

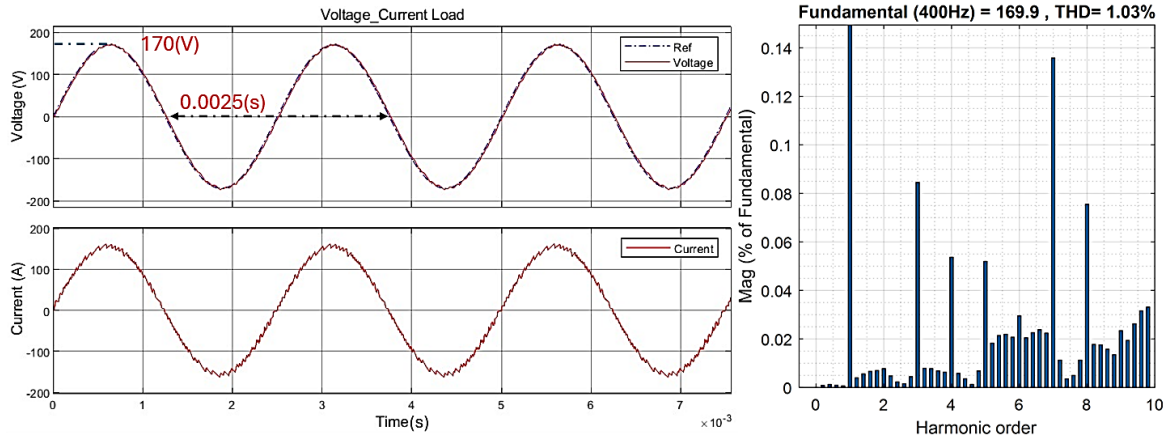


Figure 6. Voltage, current, and THD content under the linear load condition

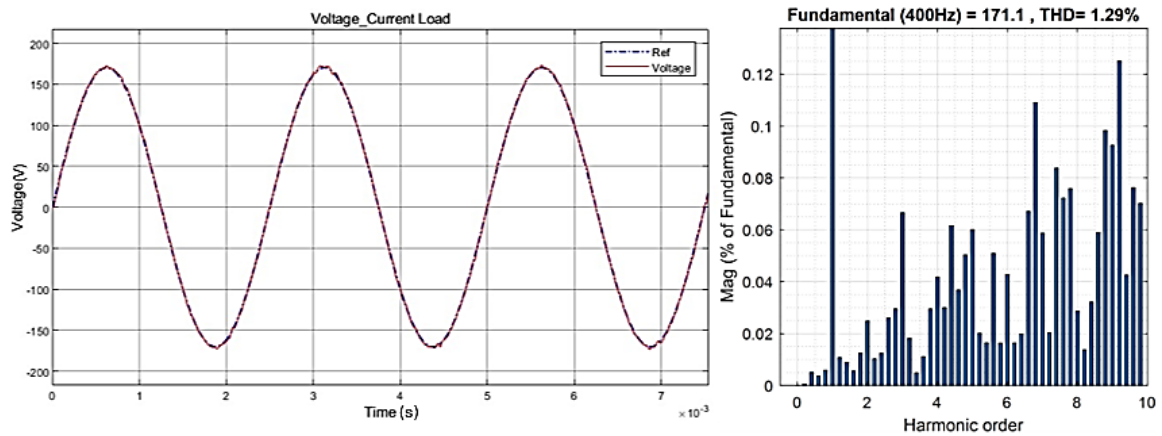


Figure 7. Output voltage and THD content under the no-load condition

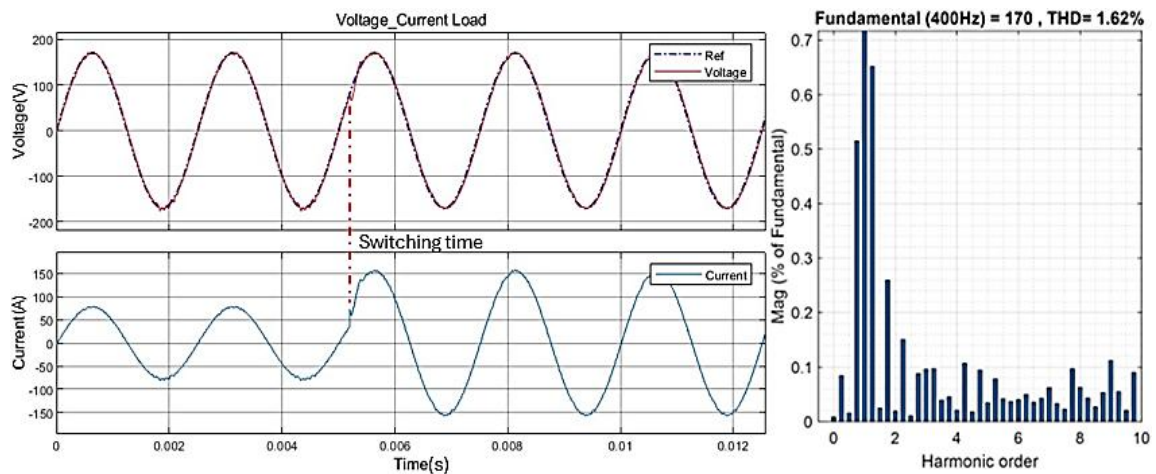


Figure 8. Output voltage and THD content under the switching load condition

The MATLAB simulation is also set up for the case of a nonlinear load, which includes a full-bridge diode rectifier with a 1.09Ω resistive load connected to a $25\mu\text{F}$ filter capacitor at the output. As shown in Figure 9, the output voltage reaches the reference value in just 0.05 s. The output voltage is maintained at 2.37%, which is within the 2.5% requirement specified by the ISO standard. With the inclusion of a 3rd harmonic compensator, the 3rd harmonic component is reduced to under 1%. However, the 5th and 7th harmonic

components remain relatively high, leading to a slight deviation in the output waveform near the zero-crossing point. This harmonic distortion can be further compensated by designing higher-order harmonic compensators in the voltage control loop.

The results under battery overcurrent due to an overload are shown in Figure 10. The scenario simulates a 200% overload condition occurring from 0.05s to 0.06s, which causes a short-time overcurrent. The results reveal the fast response of the MPC controller in limiting the current. Even though the output voltage drops to a low level for around three cycles, it remains continuous. The recovery time in this case depends on the magnitude of the overcurrent.

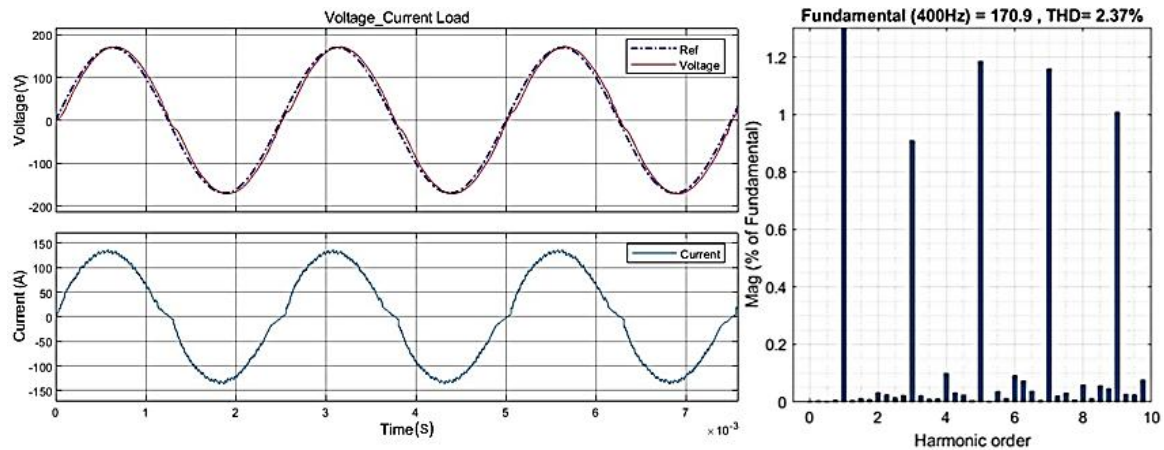


Figure 9. Output voltage and THD content under the nonlinear load condition

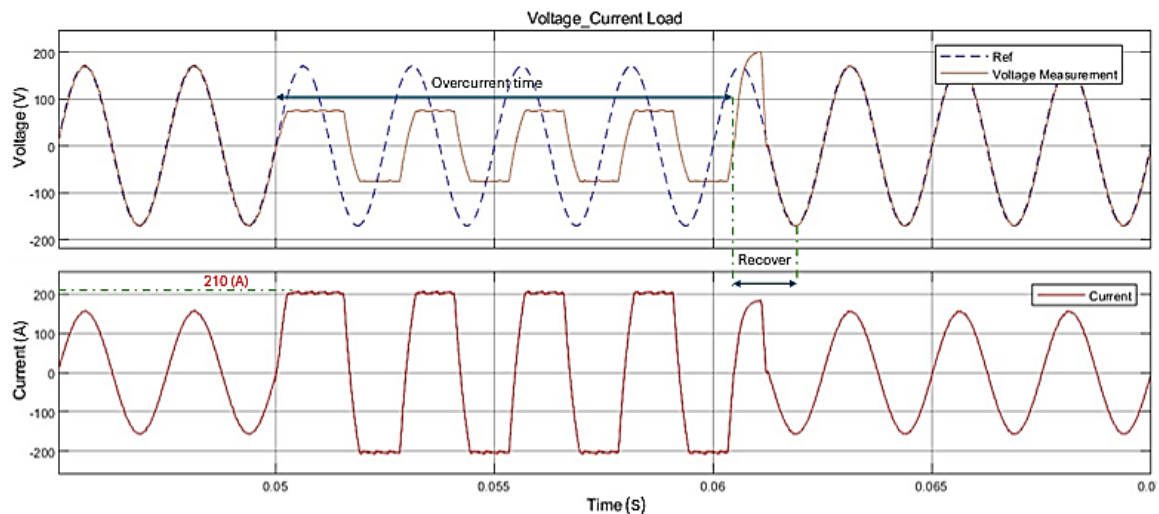


Figure 10. Output voltage and current under the short-time overcurrent condition

Finally, the proposed control system is evaluated in the case of a short-circuit fault at the output, which leads to a dramatic increase in the inductor current. In response, the MPC controller rejects all switching states that would cause the inductor current, and consequently the DC battery current, to exceed the threshold value. As shown in Figure 11, the output voltage waveform is distorted during the overcurrent period, but it remains continuous. The DC battery current is limited at the value below 130 A as depicted in Figure 12. This validates the effectiveness of the proposed control system in handling short-circuit conditions effectively.

HIL simulations the proposed control system performance is next evaluated through a real-time system by utilizing a Typhoon HIL device. The setup for the HIL simulation is illustrated in Figure 13. The first HIL simulation is conducted for the case of a linear load. As shown in Figure 14, the output voltage deviations are almost negligible, and the THD content is maintained at a remarkably low level of 1.66%, indicating a high-quality output voltage. The harmonic components are small, so harmonic compensators are not necessary in this linear load scenario.

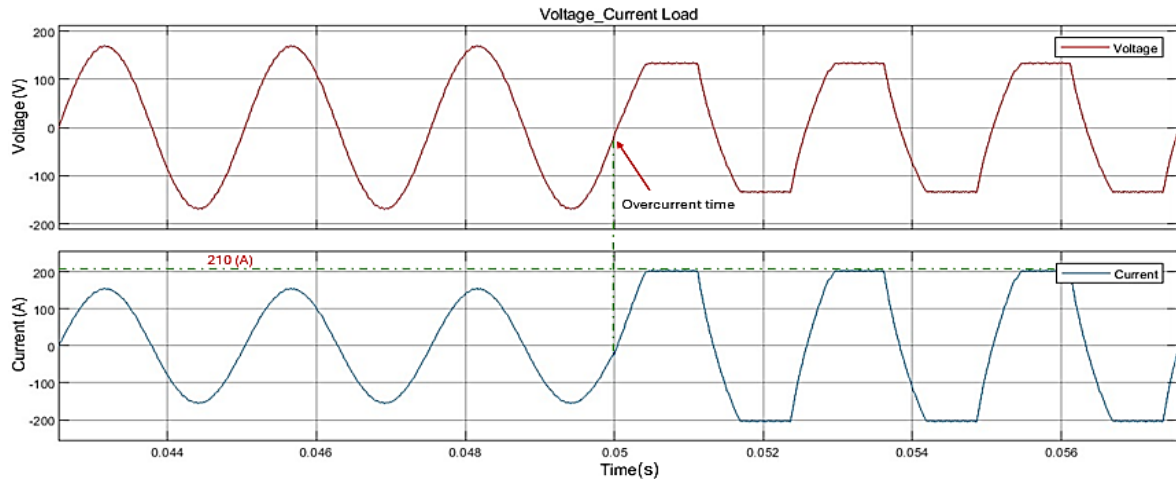


Figure 11. Output voltage and current under the battery overcurrent condition

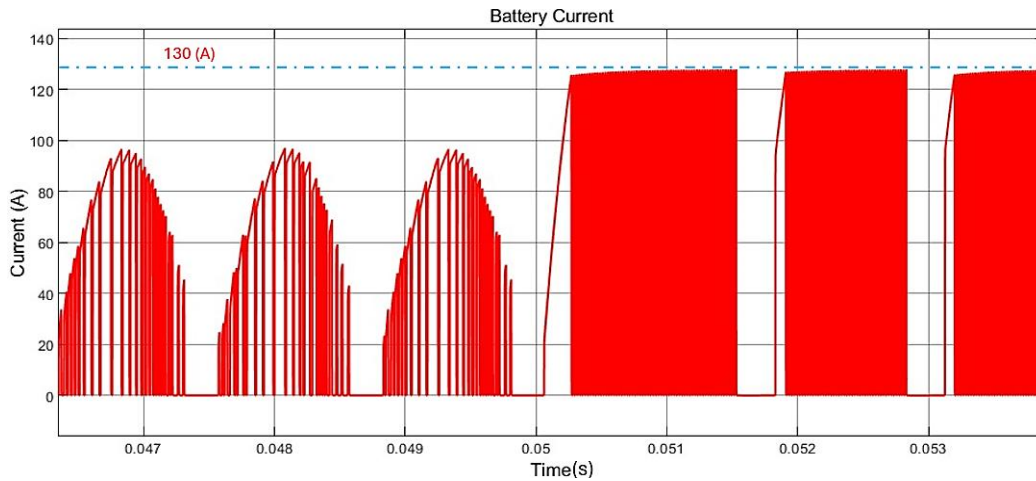


Figure 12. DC battery current has been limited under short-circuit condition

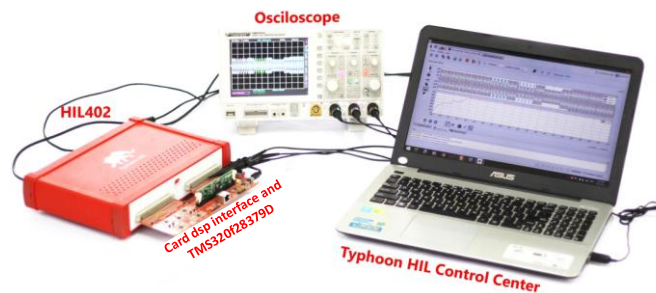


Figure 13. Typhoon HIL simulation setup

Figure 15 shows the simulation results under nonlinear load conditions, represented by a diode bridge rectifier in connection with a filter capacitance $50 \mu\text{F}$, supplying a resistive load. With the 3rd harmonic compensation is in use, the output THD now is up to 1.73%, which still satisfies the design requirement. Harmonic distortion can be seen in output voltage, but just a little, the waveform is considerably sinusoidal.

Finally, the system's response in the case of a short circuit is simulated and verified. In the scenario where a short-circuit occurs at the load side, the inductor current will increase rapidly, along with the DC current drawn from the Lithium-ion battery source, which will also rise to a large value. As can be observed in Figures 16 and 17, the MPC controller optimizes the battery current, acting to eliminate the switching states that would

cause the DC current to increase beyond the allowable threshold, and selects the optimal switching states to optimize the objective function, limiting the inductor current, and thereby restricting the DC current drawn from the battery to a value below the threshold value. Figure 18 shows the continuity of the output voltage, even though a short-circuit, the power supply is not interrupted, and the output voltage is maintained at a minimum value until the system is restored to normal operation when the short circuit fault is cleared, significantly improving the system's operating performance and confirming the superiority of the proposed control structure.

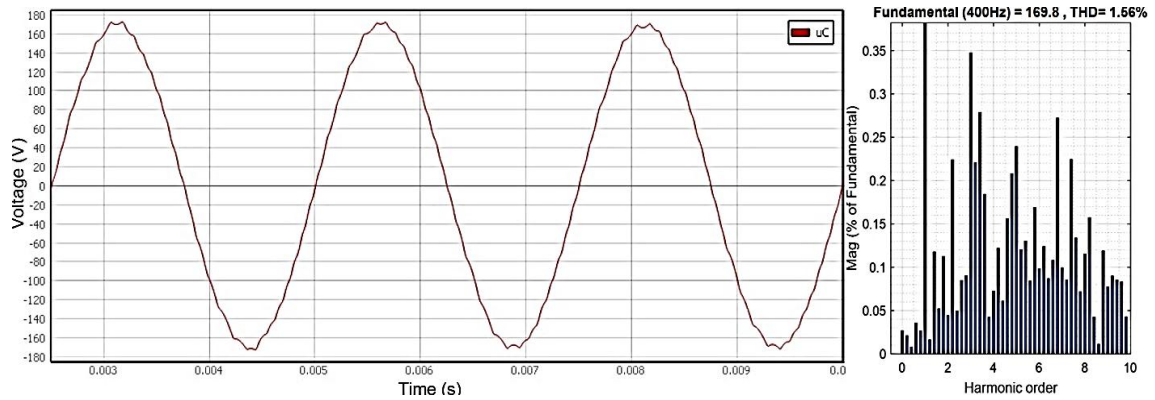


Figure 14. Output voltage and THD results under the linear load

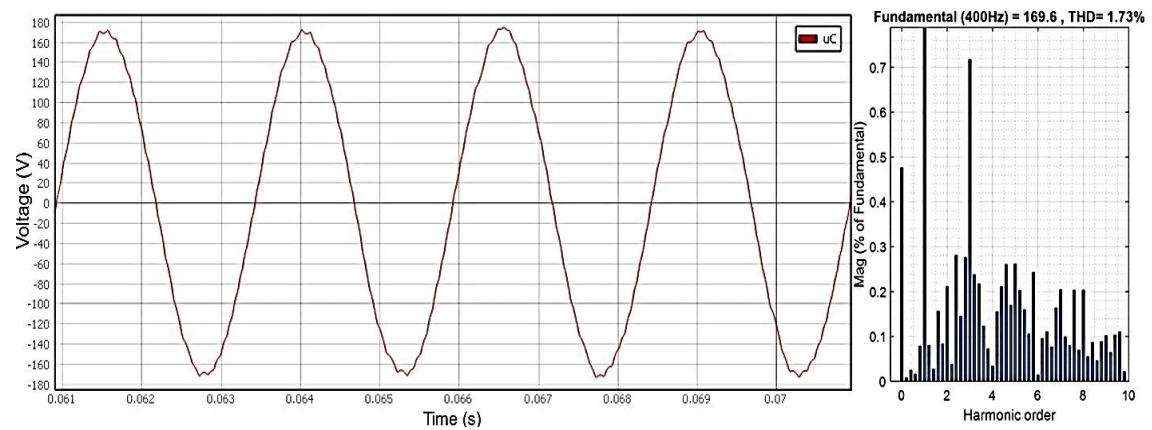


Figure 15. Output voltage and THD results under the nonlinear load

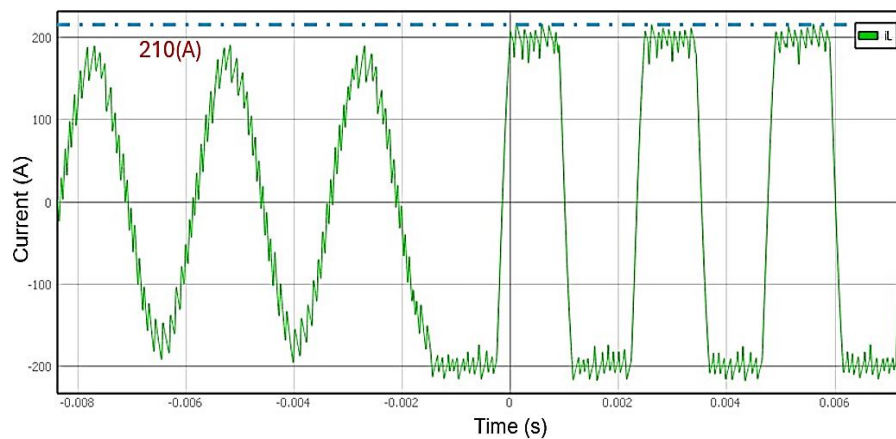


Figure 16. Inductor current under load side short-circuit condition

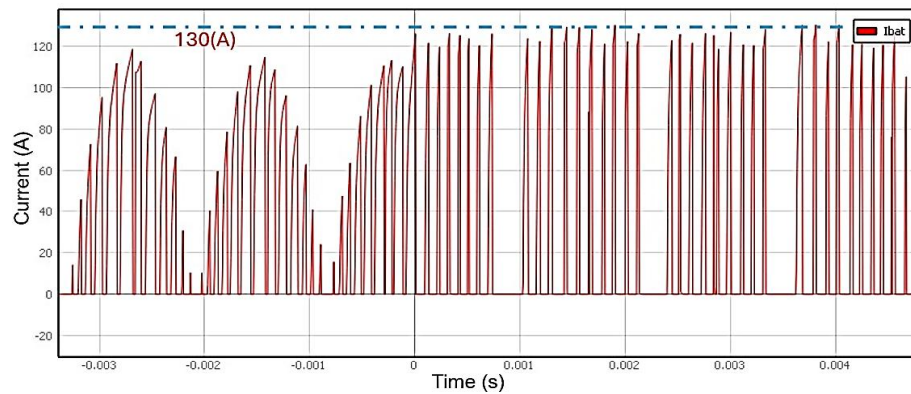


Figure 17. DC battery current under load side short-circuit condition

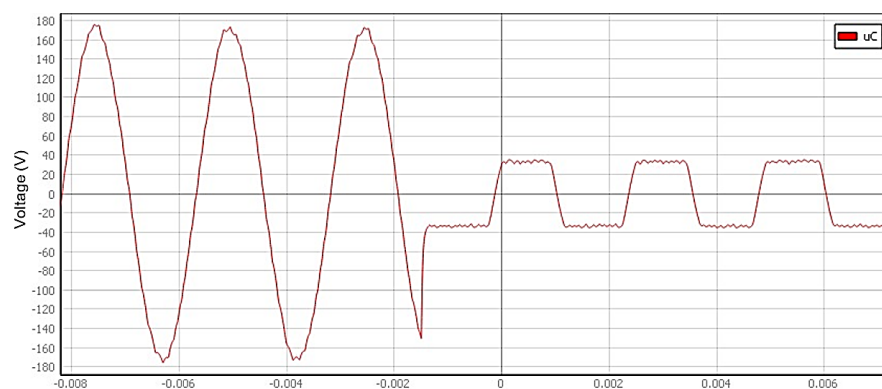


Figure 18. Output voltage remained continuous even under the load side short-circuit condition

5. CONCLUSION

A novel cascade loop control design is proposed for a Lithium-battery-powered 400 Hz GPU, in this paper. Specifically, the inner current control loop is designed using the MPC algorithm, with the main objective of limiting the DC current drawn from the lithium battery system, through the stabilization of the inductor current, which ensures the maintenance of a continuous output voltage, even in the event of overcurrent or short-circuit at the load side, thereby improving the quality of the power supply. To achieve this, an equation representing the relationship between the inductor current and the input DC current is established. An extended cost function is introduced to select the switching states that balance the minimization of the inductor current error and the limitation of the DC current within the allowable threshold. The PR control algorithm is selected for the outer voltage control loop, due to its effectiveness in stabilizing the output voltage, especially in the presence of harmonic distortion caused by nonlinear loads. The simulation results performed in MATLAB and HIL platforms prove the effectiveness of the proposed control system.

ACKNOWLEDGEMENTS

The authors wish to thank Thai Nguyen University of Technology for supporting this work.




REFERENCES

- [1] "Aircraft – Ground support electrical supplies – General requirements," International Organization for Standardization.
- [2] S. T. Que, H. Van Diep, N. Q. Dich, and N. K. Trung, "A novel 3D-space vector modulation for three single-phase combined 400Hz ground power unit," in *Proceedings - 12th IEEE International Conference on Control, Automation and Information Sciences, ICCAIS 2023*, 2023, pp. 254–259, doi: 10.1109/ICCAIS59597.2023.10382287.
- [3] L. Zheng, J. Zhu, G. Wang, D. D. C. Lu, and T. He, "Lithium-ion battery instantaneous available power prediction using surface lithium concentration of solid particles in a simplified electrochemical model," *IEEE Transactions on Power Electronics*, vol. 33, no. 11, pp. 9551–9560, 2018, doi: 10.1109/TPEL.2018.2791965.
- [4] M. Nizam, H. Maghfiroh, R. A. Rosadi, and K. D. U. Kusumaputri, "Design of battery management system (BMS) for lithium iron phosphate (LFP) battery," in *ICEVT 2019 - Proceeding: 6th International Conference on Electric Vehicular Technology 2019*, 2019, pp. 170–174, doi: 10.1109/ICEVT48285.2019.8994002.




- [5] S. Rahimifard, R. Ahmed, and S. Habibi, "Interacting multiple model strategy for electric vehicle batteries state of charge/health/power estimation," *IEEE Access*, vol. 9, pp. 109875–109888, 2021, doi: 10.1109/ACCESS.2021.3102607.
- [6] S. Hansen *et al.*, "Reliability of silicon battery technology and power electronics based energy conversion," *IEEE Power Electronics Magazine*, vol. 8, no. 2, pp. 60–69, 2021, doi: 10.1109/MPEL.2021.3075756.
- [7] K. Yu, H. Wang, L. Mao, Q. He, and Q. Wu, "IC curve-based lithium-ion battery SOC estimation at high rate charging current," *IEEE Transactions on Instrumentation and Measurement*, vol. 71, 2022, doi: 10.1109/TIM.2022.3160554.
- [8] M. Wu, L. Wang, Y. Wang, and J. Wu, "State of charge estimation of the lithium-ion power battery based on a multi-time-scale improved adaptive unscented Kalman Filter," *IEEE Transactions on Instrumentation and Measurement*, vol. 73, pp. 1–12, 2024, doi: 10.1109/TIM.2024.3390162.
- [9] X. Zhu, Z. Sun, Z. Wang, H. Wang, N. Lin, and C. Shan, "Thermal runaway in commercial lithium-ion cells under overheating condition and the safety assessment method: Effects of SoCs, cathode materials and packaging forms," *Journal of Energy Storage*, vol. 68, p. 107768, Sep. 2023, doi: 10.1016/j.est.2023.107768.
- [10] X. Lin *et al.*, "Online parameterization of lumped thermal dynamics in cylindrical lithium ion batteries for core temperature estimation and health monitoring," *IEEE Transactions on Control Systems Technology*, vol. 21, no. 5, pp. 1745–1755, 2013, doi: 10.1109/TCST.2012.2217143.
- [11] H. Perez, N. Shahmohammadhamedani, and S. Moura, "Enhanced performance of Li-ion batteries via modified reference governors and electrochemical models," *IEEE/ASME Transactions on Mechatronics*, vol. 20, no. 4, pp. 1511–1520, 2015, doi: 10.1109/TMECH.2014.2379695.
- [12] J. Jaguemont, D. Karimi, and J. Van Mierlo, "Investigation of a passive thermal management system for lithium-ion capacitors," *IEEE Transactions on Vehicular Technology*, vol. 68, no. 11, pp. 10518–10524, 2019, doi: 10.1109/TVT.2019.2939632.
- [13] M. Monfared, S. Golestan, and J. M. Guerrero, "Analysis, design, and experimental verification of a synchronous reference frame voltage control for single-phase inverters," *IEEE Transactions on Industrial Electronics*, vol. 61, no. 1, pp. 258–269, 2014, doi: 10.1109/TIE.2013.2238878.
- [14] Z. Li, Y. Li, P. Wang, H. Zhu, C. Liu, and F. Gao, "Single-loop digital control of high-power 400-Hz ground power unit for airplanes," *IEEE Transactions on Industrial Electronics*, vol. 57, no. 2, pp. 532–543, 2010, doi: 10.1109/TIE.2009.2033490.
- [15] P. W. Wheeler, P. Zanchetta, S. L. Arevalo, and W. M. Rohouma, "Repetitive control for a four leg matrix converter," in *5th IET International Conference on Power Electronics, Machines and Drives (PEMD 2010)*, Institution of Engineering and Technology, 2010, pp. 324–324, doi: 10.1049/cp.2010.0208.
- [16] S. J. Chiang, T. L. Tai, and T. S. Lee, "Variable structure control of UPS inverters," *IEE Proceedings: Electric Power Applications*, vol. 145, no. 6, pp. 559–567, 1998, doi: 10.1049/ip-epa:19982334.
- [17] O. Kukrer, H. Komurcugil, and A. Doganalp, "A three-level hysteresis function approach to the sliding-mode control of single-phase UPS inverters," *IEEE Transactions on Industrial Electronics*, vol. 56, no. 9, pp. 3477–3486, 2009, doi: 10.1109/TIE.2009.2016512.
- [18] H. Komurcugil, "Rotating-sliding-line-based sliding-mode control for single-phase UPS inverters," *IEEE Transactions on Industrial Electronics*, vol. 59, no. 10, pp. 3719–3726, 2012, doi: 10.1109/TIE.2011.2159354.
- [19] S. M. Cherati, N. A. Azli, S. M. Ayob, and A. Mortezaei, "Design of a current mode PI controller for a single-phase PWM inverter," *2011 IEEE Applied Power Electronics Colloquium, IAPEC 2011*, pp. 180–184, 2011, doi: 10.1109/IAPEC.2011.5779864.
- [20] D. Manohar and P. N. Seema, "Deadbeat controller with phase corrector for 400-Hz inverter used in ground power units of aircrafts," in *Proceedings of IEEE International Conference on Technological Advancements in Power and Energy, TAP Energy 2015*, 2015, pp. 127–131, doi: 10.1109/TAPENERGY.2015.7229604.
- [21] M. Nouri, O. Salari, K. Hashtrudi-Zaad, and A. Bakhshai, "A hybrid designed digital dual-loop control of high power ground power unit (GPU)," in *2017 19th European Conference on Power Electronics and Applications, EPE 2017 ECCE Europe*, 2017, doi: 10.23919/EPE17ECCEEurope.2017.8099172.
- [22] H. W. Lee, T. Y. Yoon, and K. B. Lee, "Model predictive control with space vector modulation based on a voltage angle for driving open-end winding IPMSM," *IEEE Access*, vol. 12, pp. 89026–89034, 2024, doi: 10.1109/ACCESS.2024.3419724.
- [23] Y. Wang *et al.*, "A Novel extended sliding-mode predictive control with dynamic optimization and virtual voltage vectors," *IEEE Transactions on Power Electronics*, vol. 39, no. 9, pp. 10976–10988, 2024, doi: 10.1109/TPEL.2024.3411565.
- [24] A. Abdelaleem, A. I. M. Ali, M. Nasrallah, E. E. M. Mohamed, H. S. Hussein, and M. A. Ismeil, "Model predictive control for single-stage three-phase split source inverter with enhanced switched-inductor configuration," *IEEE Access*, vol. 12, pp. 60782–60796, 2024, doi: 10.1109/ACCESS.2024.3394737.
- [25] E. Zafra, S. Vazquez, T. Geyer, R. P. Aguilera, E. Freire, and L. G. Franquelo, "Computational analysis of the long horizon FCS-MPC problem for power converters," *IEEE Transactions on Power Electronics*, vol. 39, no. 10, pp. 12762–12773, Oct. 2024, doi: 10.1109/TPEL.2024.3419060.
- [26] D. Limon, T. Alamo, F. Salas, and E. F. Camacho, "On the stability of constrained MPC without terminal constraint," *IEEE Transactions on Automatic Control*, vol. 51, no. 5, pp. 832–836, 2006, doi: 10.1109/TAC.2006.875014.
- [27] R. Dubay and M. Abu-Ayyad, "Properties of extended predictive control," *ISA Transactions*, vol. 46, no. 1, pp. 103–111, Feb. 2007, doi: 10.1016/j.isatra.2006.06.004.
- [28] D. Stenger, R. Ritschel, F. Krabbes, R. Voßwinkel, and H. Richter, "What is the best way to optimally parameterize the MPC cost function for vehicle guidance?," *Mathematics*, vol. 11, no. 2, p. 465, Jan. 2023, doi: 10.3390/math11020465.
- [29] Y. Chen, X. Wang, X. Meng, M. He, D. Xiao, and Z. Wang, "A universal model predictive control strategy for dual inverters fed OW-PMSM drives," *IEEE Transactions on Power Electronics*, vol. 38, no. 6, pp. 7575–7585, Jun. 2023, doi: 10.1109/TPEL.2023.3260305.
- [30] B. Long *et al.*, "Passivity-based partial sequential model predictive control of T-Type grid-connected converters with dynamic damping injection," *IEEE Transactions on Power Electronics*, vol. 38, no. 7, pp. 8262–8281, Jul. 2023, doi: 10.1109/TPEL.2023.3266588.
- [31] J. Han, H. Yuan, W. Li, L. Zhou, C. Deng, and M. Yan, "FCS-MPC based on dimension unification cost function," *Energies*, vol. 17, no. 11, p. 2479, May 2024, doi: 10.3390/en17112479.
- [32] F. Rojas, R. Cardenas, J. Clare, M. Diaz, J. Pereda, and R. Kennel, "A design methodology of multiresonant controllers for high performance 400 Hz ground power units," *IEEE Transactions on Industrial Electronics*, vol. 66, no. 8, pp. 6549–6559, 2019, doi: 10.1109/TIE.2019.2898610.
- [33] A. A. Nazeri, P. Zacharias, F. M. Ibanez, and S. Somkun, "Design of proportional-resonant controller with zero steady-state error for a single-phase grid-connected voltage source inverter with an LCL output filter," *2019 IEEE Milan PowerTech, PowerTech 2019*, 2019, doi: 10.1109/PTC.2019.8810554.
- [34] D. Mu, J. Jiang, and C. Zhang, "Online semiparametric identification of lithium-ion batteries using the wavelet-based partially linear battery model," *Energies*, vol. 6, no. 5, pp. 2583–2604, 2013, doi: 10.3390/en6052583.

BIOGRAPHIES OF AUTHORS






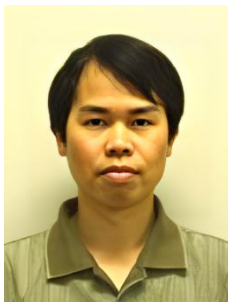
Son Tran Que    was born in Thai Nguyen, Vietnam. He received the B.E. and M.Sc. degrees in Electrical Engineering from Thai Nguyen University of Technology, Vietnam in 2010 and 2015, respectively. From 2010, he works as a lecturer at Thai Nguyen University of Technology. His current research interests include high-frequency converters and automatic control. He can be contacted at email: tranqueson.ktdt@tnut.edu.vn.






Vuong Nguyen Anh    was born on 2002, in Nghe An, Viet Nam. He is currently a student majoring in industrial automation at Ha Noi University of Science and Technology. His current research interests include power electronics and electric drive control. He can be contacted at email: nguyenanhvuong001@gmail.com.






Diep Huynh Van    was born on 2002, in Thai Nguyen, Viet Nam. He is currently a student majoring in industrial automation at Ha Noi University of Science and Technology. His current research interests include power electronics and electric drive control. He can be contacted at email: huynhdiep17k@gmail.com.



Dich Nguyen Quang    was born in Bac Ninh, Vietnam. He received the B.Sc. degree in electrical engineering from Hanoi University of Technology, Hanoi, Vietnam, in 1997, and the M.Sc. degree in electrical engineering from Dresden University of Technology, Dresden, Germany, in 2003. In 2010, he received the Ph.D. degree at Ritsumeikan University, Kusatsu, Japan. In 2000, he joined the Department of Industrial Automation, Hanoi University of Technology. His current research interests include magnetic bearings, self-bearing motors, and sensorless motor control. He can be contacted at email: dich.nguyenquang@hust.edu.vn.



Trung Nguyen Kien    was born in Hanoi, Vietnam. He received the B.E. and M.Sc. degrees in control and automation from Hanoi University of Science and Technology, Vietnam in 2008 and 2011, respectively. In 2016, he received a Ph.D. degree in Functional control systems at Shibaura Institute of Technology, Japan, where he worked as a postdoctoral researcher from 2016-2017. In 2008, he joined the Department of Industrial Automation, at Hanoi University of Science and Technology. His current research interests include a high-frequency converters, battery charging technology for EVs, battery management systems, and wireless power transfer systems. He can be contacted at email: trung.nguyenkien1@hust.edu.vn.